NJC

PAPER

View Article Online
View Journal | View Issue

Check for updates

Cite this: *New J. Chem.*, 2021, **45**, 2696

Ligand influence *versus* electronic configuration of d-metal ion in determining the fate of NIR emission from Ln^{III} ions: a case study with Cu^{II}, Ni^{II} and Zn^{II} complexes†

Abhineet Verma,[ab] S. K. Saddam Hossain,[c] Sailaja S. Sunkari,*[b] Joseph Reibenspies[d] and Satyen Saha*[a]

Received 10th August 2020,
Accepted 28th December 2020

DOI: 10.1039/d0nj04020g

rsc.li/njc

Lanthanides (Ln^{III}) are well known for their characteristic emission in the near-infrared region (NIR). However, direct excitation of lanthanides is not feasible as described by Laporte's parity selection rule. Here, we obtain NIR emission from [**L–M–Ln**] complexes (where, L = an organic ligand, M = a d-block metal ion, and Ln = a lanthanide ion) in which the [**L–M**] moiety acts as an antenna to absorb the excitation light to transfer to Ln energy levels. Based on fifteen lanthanide complexes that are presented here in which Cu, Ni and Zn complexes with a Schiff base ligand act as an antenna, we have demonstrated for the first time that electronic configuration of the d-block metal ion is very crucial for obtaining NIR emission. With Ln ion and the same ligand, Cu and Ni complexes show completely different emission than that of the corresponding NIR emitting [**L–Zn–Ln**] complexes.

Introduction

In recent years electromagnetic radiation, specifically the near-infrared (NIR) region (650 to 1600 nm) has become popular among researchers working in materials and biosciences.[1] Lanthanide (Ln^{III}) ions are well reported to emit in this region. Luminescent lanthanides can have emission bands ranging from the visible to NIR regions, controlled by the nature of the Ln^{III} ions. However, due to the fact that Ln^{III} cannot be directly excited by an external source, the requirement for indirect excitation arises.[2] Back in 1942, Weissman was the first to show that lanthanide-centred luminescence in coordination compounds can be sensitized upon ligand excitation.[3] The excitation energy that is absorbed by the coordinating ligand can subsequently be funnelled onto the excited states of lanthanide ion, which is now well known as the "antenna effect".[2] This finding eventually broadens considerably the scope of lanthanide photonics. In addition, due to forbidden parity from the f–f transitions, the absorption coefficients of these lanthanide ions are normally very low ($\varepsilon \approx 1^{-10}$ M^{-1} cm^{-1}).[1] This disadvantage is also eluded by coordinating with organic ligands or by use of organic ligand–d-block metal complexes. It is postulated that when the Ln^{III} ion is inserted into a chemical environment as in the case of Ln–organic ligand coordination complexes, several non-centrosymmetric interactions permit the mixing of electronic states of opposite parity into the 4f wave functions and induced electric dipole transitions become partially allowed.[3] Interestingly, it has been noted that the intensity of some of these bands is found to be sensitive to the nature of the environment surrounding the metal-ion, and therefore the transitions responsible for these bands are called "hypersensitive" and tunable.[3]

Emission from Ln^{III} ions is a fundamentally important process as evident from a continuously expanding range of applications starting from biology,[4] to materials for various purposes like in lasers,[4] OLEDs,[5] optical fibres,[5] and WLEDs.[5] The state of the art application has recently been reviewed extremely well by Bünzil.[6] Considering the understanding that functional properties and structural aspects of living systems are the key challenges in biology and medicine, NIR emitting materials have recently been found to be promising in the application of biological cell imaging. Besides the biological imaging, NIR luminescent materials (particularly, Er, Nd and Ho) are found to be useful for telecommunication, as the active material for optical amplification of the NIR signal,[7] and

[a] *Department of Chemistry, Institute of Science, Banaras Hindu University, Varanasi, India. E-mail: satyen.saha@gmail.com*
[b] *Department of Chemistry, Mahila Maha Vidhyalaya, Banaras Hindu University, Varanasi, India. E-mail: sunkari.s7@gmail.com*
[c] *School of Chemistry, University of Hyderabad, Hyderabad, India*
[d] *X-ray Diffraction Laboratory, Department of Chemistry, Texas A&M University, USA. E-mail: reibenspies@chem.tamu.edu*

† Electronic supplementary information (ESI) available. CCDC 1913571, 1891364, 2021619, 1891363, 1891365, 1480671, 1480672, 1480673, 1918470 and 1918455. For ESI and crystallographic data in CIF or other electronic format see DOI: 10.1039/d0nj04020g

encrypted tags ("barcodes") to recognize the identity of chemical or biological samples.[5] It is important to understand that NIR luminescent materials possess several critical advantages over semiconductor nanocrystals,[5,7,8] carbon nanotubes[9] and organic fluorophores[7] due to having multiple sharp emission bands in addition to photostability and longer luminescence lifetimes. As already discussed, the wavelength of sharp emissions, as well as the intensities, can be tuned by varying the environment in which Ln^{III} ions are embedded. One of the popular ways is to use organic ligands to make a complex with Ln^{III} ions. This organic ligand acts as an antenna to absorb the excitation light and then passes the absorbed energy onto the energy manifold of Ln ions. Since light of longer wavelength is used as an excitation source for various applications, it is necessary to find chromophores that absorb at a longer wavelength. Due to scarcity of suitable chromophores that can coordinate with Ln^{III} ions, a popular method has been developed to use organic ligand–d-block metal complexes as the 'antenna'. It can be seen that especially metal ions having d^{10} configuration leads to the formation of complexes with a large molar absorption coefficient, resulting in better-sensitized emission.[10] It can be seen in the literature that Zn^{II} is quite frequently used for this type of complex formation over any other d-block metal ion.[11,42] Limited literature is available which depicts that complexes of d-block metal ions having configurations other than d^{10}, do not show good emission intensities.[7,41] Among them, Cu^{II}, in particular, is reported for its malign behaviour as it quenches the fluorescence.[7,43] However, to the best of our knowledge, there is no literature where systematic studies have been performed with the same set of organic ligands complexed to various d-block metal ions including Zn^{II} ion, as an antenna for Ln^{III} ion emission, to study the effect of d-configuration on the photophysical responses of Ln^{III} complexes.

To understand the importance of Zn^{II} ion on the antenna effect, we have synthesized three series of Cu^{II}, Ni^{II} and Zn^{II} ion complexes with the same organic ligand and used those complexes as an antenna to complex with several Ln^{III} ions (Nd, Pr, Sm, Dy, and Er). All the complexes, except for the Ni^{II} series (due to nonformation of single crystals) were structurally characterized by the single-crystal X-ray diffraction (SCXRD) technique. Rietveld's method[12] was successfully applied for determination of the structure for all Ni^{II} complexes from the PXRD data. Comparative NIR luminescence studies of these complexes are reported herein with an intention to understand the effect of d electronic configuration on the final luminescence of several Ln-complexes.

Experimental section

Material and methods

3-Methoxysalicylaldehyde, 1,4-diamino-butane, $Ni(CH_3COO)_2 \cdot 2H_2O$, $Cu(CH_3COO)_2 \cdot H_2O$, $Zn(CH_3COO)_2 \cdot 2H_2O$ and $Ln(NO_3)_3 \cdot 6H_2O$ were purchased from Sigma Aldrich and were used without further purification. Infrared spectra were recorded on a PerkinElmer Spectrum-2 FTIR spectrometer using KBr pellets in the region of 400–4000 cm^{-1}. The powder X-ray diffraction (PXRD) data were collected on a Bruker D8-ADVANCE diffractometer equipped with Cu Kα1 (λ = 1.5406 Å; 1600 W, 40 kV, 40 mA) at a scan speed of 5° min^{-1}. Rietveld's method[12] was successfully applied for determination of the quantitative phases of all [**L–Ni–Ln**] complexes. Rietveld refinement has been done by adjusting major parameters: scale factor, flat background, zero-point shift, lattice parameters, orientation parameters, peak width parameters, asymmetry parameter and peak shape. Initial guess parameters have been taken from corresponding single crystal data of Zn complexes. Peak profiles were fitted with the pseudo-Voigt function.[13] Elemental analyses were measured on a Vario EL III elemental analyzer. A diffractometer was employed for crystal screening, unit cell determination, and data collection. The crystal mounted on a nylon loop was then placed in a cold nitrogen stream (Oxford) maintained at 110 K. 45 data frames were taken at widths of 1°. These reflections were used to determine the unit cell. The unit cell was verified by examination of the *hkl* overlays on several frames of data. After careful examination of the unit cell, an extended data collection procedure (5 sets) was initiated using omega and phi scans. The goniometer was controlled using the APEX3 software suite.[14] The sample was optically centered with the aid of a video camera such that no translations were observed as the crystal was rotated through all positions. The X-ray radiation employed was generated from a Mo–I μs X-ray tube (Kα = 0.71073 Å). Integrated intensity information for each reflection was obtained by reduction of the data frames using the program APEX3.[14] The integration method employed a three-dimensional profiling algorithm, and all data were corrected for Lorentz and polarization factors, as well as for crystal decay effects. Finally, the data were merged and scaled to produce a suitable data set. The absorption correction program SADABS[15] was employed to correct the data for absorption effects. Crystal data for complexes [**C1** to **C5**] were collected on a Bruker CMOS area detector with a microfocus sealed X-ray tube as a source using graphite monochromatized Mo-Kα radiation at 173 K, for [**C1**], at 110 K for complexes [**C2** to **C4**] and at 100 K for [**C5**]. Data for complexes [**Z1** to **Z3**] were collected on an OXFORD DIFFRACTION XCALIBER EoS diffractometer using graphite monochromatized Mo-Kα radiation at 298 K and for [**Z4** and **Z5**], on a Rigaku Saturn724 using a rotating anode as a X-ray generator, and Mo-Kα radiation at 293 K. Electronic spectra were recorded on a CARY 100 BIO UV-vis spectrophotometer. Fluorescence spectra were recorded on a Horiba spectrofluorometer (Fluoromax).

Results and discussion

Preparation of lanthanide complexes

All the complexes were synthesized in a similar manner (Scheme 1), except for the change in metal ions. A typical procedure is detailed here, for complex [**L–Ni**] with Nd, while only analytical details are provided for the rest.

Ligand synthesis (L). The synthesis of ligand **L** is done following the procedure described elsewhere,[16] where 1 mole of 1,4-diamino butane was condensed with 2 moles of *o*-vanillin under reflux conditions in ethanol.

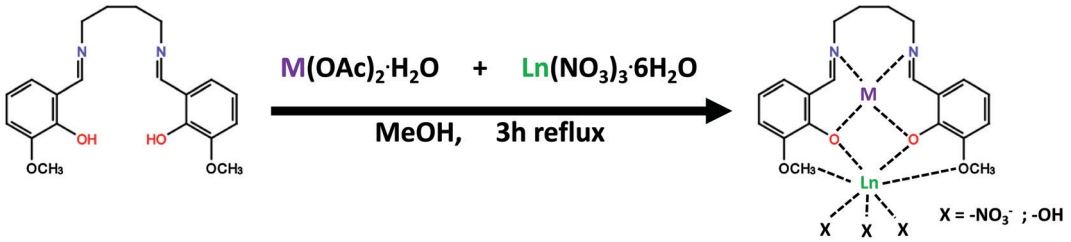

Ni Complexes (Ln)	Cu Complexes (Ln)	Zn Complexes (Ln)
N1 : Nd	C1 : Nd	Z1 : Nd
N2 : Pr	C2 : Pr	Z2 : Pr
N3 : Sm	C3 : Sm	Z3 : Sm
N4 : Dy	C4 : Dy	Z4 : Dy
N5 : Er	C5 : Er	Z5 : Er

Scheme 1 Synthetic route for the preparation of the complexes. M stands for d-block metal ion, while Ln stands for lanthanide ion. MeOH represents methanol.

[N1]. 20 mL of a methanolic solution of ligand (**L**) (0.38 g, 1.0 mmol) was added to 15 mL of methanolic solution of $Ni(CH_3COO)_2{\cdot}2H_2O$ (0.43 g, 1.0 mmol) while stirring, followed by dropwise addition of 15 mL of a methanolic solution of $Nd(NO_3)_3{\cdot}6H_2O$ (0.10 g, 1.0 mmol). The mixture was refluxed for 3 hours, cooled to room temperature and filtered. Layer diffusion of ether into the methanolic filtrate at moderate temperature (~15 to 20 °C) afforded (i) dark greenish-black coloured powder for [**L–Ni–Ln**] complexes; (ii) shiny black coloured plate-shaped crystals for [**L–Cu–Ln**] and (iii) light yellow blocks for [**L–Zn–Ln**] complexes, suitable for SCXRD measurements.

Yields for [**N1**]: 0.80 g (1.5 mmol, 87.9%); M.P. 270.0 (±1) °C; anal. calcd for $C_{23}H_{29}N_4O_{13}NiNd$ (M.W. = 771.39): C 35.76; H 3.78; N 7.25. Found C 35.52; H 3.41; N 7.43. [**N2**]: 0.65 g (0.9 mmol, 71.4%); M.P. 273.9 (±1) °C; anal. calcd for $C_{23}H_{29}N_4O_{13}NiPr$ (M.W. = 768.06): C 35.92; H 3.80; N 7.28. Found C 35.91; H 3.42; N 7.32. [**N3**]: 0.35 g (0.5 mmol, 38.5%); M.P. 274.3 (±1) °C; anal. calcd for $C_{23}H_{29}N_4O_{13}NiSm$ (M.W. = 778.52): C 35.48; H 3.75; N 7.20. Found C 35.18; H 3.42; N 7.23. [**N4**]: 0.46 g (0.6 mmol, 50.5%); M.P. 283.1 (±1) °C; anal. calcd for $C_{22}H_{25}N_4O_{12}NiDy$ (M.W. = 758.62): C 34.83; H 3.32; N 7.39. Found C 35.12; H 3.39; N 7.12. [**N5**]: 0.31 g (0.4 mmol, 34.1%); M.P. 286.3 (±1) °C; anal. calcd for $C_{22}H_{25}N_4O_{12}NiEr$ (M.W. = 763.38): C 34.61; H 3.30; N 7.34. Found C 34.51; H 3.68; N 7.12.

[C1]. 0.76 g (1.4 mmol, 83.5%); M.P. 275.3 (±1) °C; anal. calcd for $C_{20}H_{22}N_5O_{13}CuNd$ (M.W. = 748.17): C 32.10; H 2.96; N 9.36. Found C 32.21; H 3.01; N 10.10. [**C2**]: 0.70 g (0.9 mmol, 76.9%); M.P. 271.2 (±1) °C; anal. calcd for $C_{20}H_{22}N_5O_{13}CuPr$ (M.W. = 744.87): C 32.25; H 2.98; N 9.40. Found C 32.31; H 2.83; N 9.83. [**C3**]: 0.66 g (0.9 mmol, 72.5%); M.P. 271.8 (±1) °C; anal. calcd for $C_{20}H_{22}N_5O_{13}CuSm$ (M.W. = 754.29): C 31.84; H 2.94; N 9.28. Found C 32.11; H 3.31; N 9.10. [**C4**]: 0.60 g (0.8 mmol, 65.93%); M.P. 276.5 (± 1) °C; anal. calcd for $C_{20}H_{22}N_5O_{13}CuDy$ (M.W. = 766.43): C 31.34; H 2.89; N 9.14. Found C 31.10; H 2.99; N 9.57. [**C5**]: 0.72 g (0.9 mmol, 79.1%); M.P. 270.0 (±1) °C; anal. calcd for $C_{20}H_{22}N_5O_{13}CuEr$ (M.W. = 771.19): C 31.15; H 2.88; N 9.08. Found C 31.21; H 3.03; N 8.92.

[Z1]. 0.89 g (1.1 mmol, 89.3%); M.P. 261.8 (± 1) °C; anal. calcd for $C_{23}H_{29}N_4O_{13}ZnNd$ (M.W. = 778.11): C 35.50; H 3.63; N 7.20. Found C 35.65; H 3.72; N 7.25. [**Z2**]: 0.85 g (1.1 mmol, 85.5%); M.P. 269.4 (±1) °C; anal. calcd for $C_{23}H_{29}N_4O_{13}ZnPr$ (M.W. = 774.77): C 35.66; H 3.64; N 7.23. Found C 35.75; H 2.70; N 7.30. [**Z3**]: 0.76 g (1.0 mmol, 76.9%); M.P. 267.3 (±1) °C; anal. calcd for $C_{23}H_{29}N_4O_{13}ZnSm$ (M.W. = 785.23): C 35.18; H 3.72; N 7.13. Found C 36.47; H 3.75; N 7.24. [**Z4**]: 0.80 g (0.5 mmol, 80.5%); M.P. > 350.0 (±1) °C; anal. calcd for $C_{22}H_{25}N_4O_{12}ZnDy$ (M.W. = 765.33): C 34.52; H 3.29; N 7.31. Found C 34.36; H 3.32; N 7.28. [**Z5**]: 0.75 g (0.5 mmol, 75.3%); M.P. > 350.0 (±1) °C; anal. calcd for $C_{22}H_{25}N_4O_{12}ZnEr$ (M.W. = 770.09): C 34.31; H 3.27; N 7.28. Found C 34.12; H 3.31; N 7.32. FT-IR spectra of all the complexes are given in the ESI† (Fig. S1).

General characterization

Heterobimetallic complexes have been synthesized *in situ* (three different series) in a stepwise manner without the isolation of mononuclear d-block complexes. FT-IR spectra (ESI,† Fig. S1), for all fifteen complexes, exhibit a sharp peak due to the azomethine (C═N) group of the Schiff base in the range of 1615–1630 cm^{-1}.[17] The phenolic C–O stretching band at 1249 cm^{-1} in the spectra of **L** was shifted to 1217 cm^{-1} on complexation, supporting the deprotonation and coordination of the phenolic oxygen donor to the metal centre. The counter anions show their characteristic vibrational band in FT-IR spectra. Sharp bands appearing at 526 and 421 cm^{-1} correspond to the M–N and M–O stretching frequencies, respectively. [**L–Zn–Ln**] and [**L–Ni–Ln**] series have an extra band at about 1495 cm^{-1} showing the presence of the acetate group in these complexes. Other high energy bands such as the one at 920 cm^{-1} for C–C stretching in the $-(O)_2C-CH_3$ group can also be noticed.

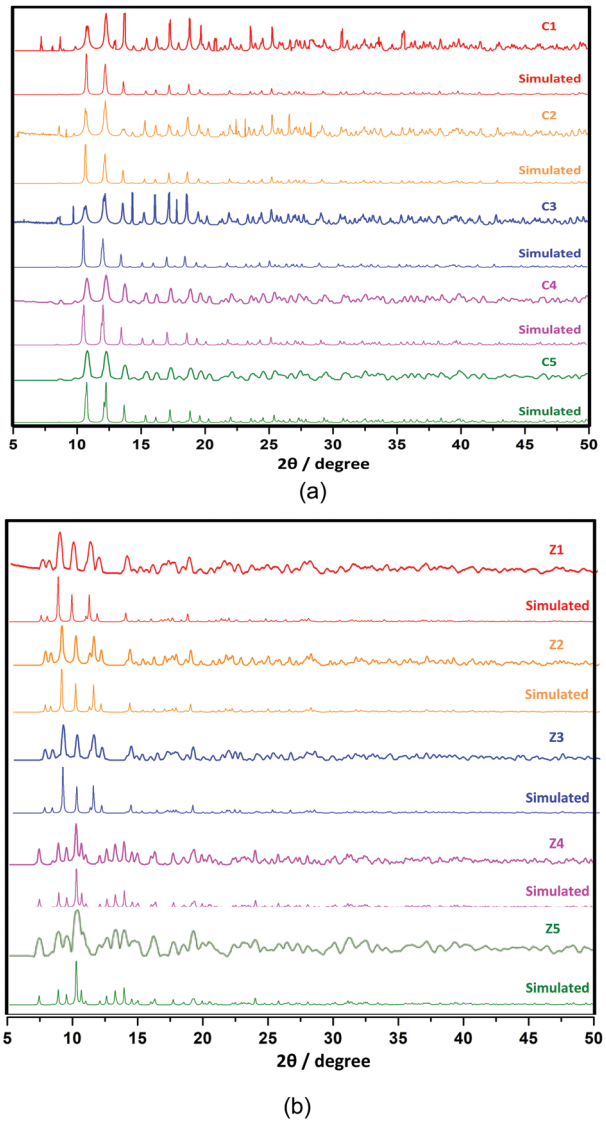

Fig. 1 PXRD patterns for the complexes (a) [**L–Cu–Ln**] and (b) [**L–Zn–Ln**]. For comparison, the simulated patterns generated from SCXRD data are also given. The patterns for [**L–Ni–Ln**] complexes are discussed separately.

Powder X-ray diffraction (PXRD) patterns (Fig. 1) confirm the bulk purity of the complexes. For [**L–Cu–Ln**] and [**L–Zn–Ln**] complexes, the experimental PXRD patterns are in good agreement with the simulated patterns obtained from the SCXRD data, indicating crystal structures are the true representative of the bulk. However, in addition, experimental PXRD data have been used to elucidate the structures for [**L–Ni–Ln**] complexes for which SCXRD data are not available. In order to determine lattice parameters and to quantify the phases present in [**L–Ni–Ln**] complexes, Rietveld refinement was carried out.[12] Fig. 4 and Fig. S4, Table S1 (ESI†) show detailed information obtained after Rietveld refinement of all [**L–Ni–Ln**] complexes. Considering the integrated intensity of the peaks as a function of structural parameters only, the Marquardt least-squares[18] procedure was used for minimization of the difference between the observed and simulated powder diffraction patterns.[19] The minimization was carried out using the reliability index parameter, R_{wp} (weighted residual error), RB (Bragg factor) and R_{exp} (expected error).[20] The determined structures are presented in the ESI,† Fig. S5. The goodness of fitting (χ^2) for [**N1**] to [**N5**] are 1.27, 1.73, 1.33 1.28 and 1.29, respectively.

SCXRD studies

Single crystal structures are solved by direct methods and refined by full matrix least-squares on F^2 using SHELX-2018.[21] The non-hydrogen atoms were refined with anisotropic thermal parameters. A disordered carbon atom of the methoxy group (C19) of complexes in [**L–Zn–Nd**], [**L–Zn–Pr**] and [**L–Zn–Sm**] is modeled by splitting into two halves with positions refined by FVAR refinement and thermal parameters by anisotropic refinement. All the hydrogen atoms are geometrically fixed and allowed to ride upon the atom to which they are attached. Important crystal data for Cu and Zn containing complexes are presented in Table 1 whereas important bond angles and bond distances are presented in Table 2. In spite of several efforts (at different temperature, with different solvent combinations as well as emplying diffusion technique) to grow the single crystals, none of the [**L–Ni–Ln**] complexes could be grown as a single crystal suitable for SCXRD measurements. However, all other crystals could be grown by employing a diffusion technique using a combination of methanol and ether solvents at laboratory temperature. Drawings are made using OLEX II,[22] ORTEP-III and MERCURY.[23,24] The refinement converged to final values of R_1 & wR_2 = 0.0291 & 0.0664 for [**C1**]; 0.0325 & 0.0734 for [**C2**]; 0.0310 & 0.0755 for [**C3**]; 0.0244 & 0.0526 [**C4**]; 0.0194 & 0.0412 for [**C5**]; 0.0809 & 0.1809 for [**Z1**]; 0.0663 & 0.1167 for [**Z2**]; 0.1067 & 0.1944 for [**Z3**]; 0.0359 & 0.0935 for [**Z4**]; and 0.0274 & 0.0705 for [**Z5**], respectively.

Each series of complexes is found to be isostructural. Complexes [**C1** to **C5**] are isostructural, crystallizing in the monoclinic system with a space group $P2_1/n$ as shown in Fig. 2. The crystallographically independent unit contains one neutral Cu^{II} and Ln^{III} heterodinuclear unit, $[Cu(\mu\text{-}L)Ln(NO_3)_2]$ [Ln^{III} = Nd for [**C1**]; Pr for [**C2**]; Sm for [**C3**]; Dy for [**C4**] & Er for [**C5**]; L = *N*,*N*′-bis(3-methoxysalicylidene)-1,4-diaminobutane]. On the other hand, complexes [**Z1** to **Z5**] are also isostructural, crystallizing in the monoclinic system but with different space groups. $P2_1/c$ for [**Z1**] and [**Z2**], $P2_1/a$ for [**Z3**] and $P2_1/n$ for [**Z4**] and [**Z5**] (Fig. 2). The crystallographically independent unit contains one neutral Zn^{II} and Ln^{III} heterodinuclear unit, $[Zn(\mu\text{-}L)(\mu\text{-}CH_3COO)SLn(NO_3)_2]$ for Ln^{III} = Nd for [**Z1**], Pr for [**Z2**] and Sm for [**Z3**] S = CH_3OH, whereas complexes [**Z4**] and [**Z5**] have two crystallographically independent units where $[Zn(\mu\text{-}L)(\mu\text{-}CH_3COO)Ln(NO_3)_3]$ for [Ln^{III} = Dy for [**Z4**] and Er for [**Z5**] L = *N*,*N*-bis(3-methoxysalicylidene)-1,4-diaminobutane].

[**L–Cu–Ln**] complexes [**C1** to **C5**] are iso-structural. Here Cu^{II} ions adopt the distorted square planar geometry occupied by two nitrogen atoms (N1 and N2) and two phenoxo oxygen (O1 and O2) atoms from the ligand; whereas the Ln^{III} ions are ten coordinated adopting a bicapped square antiprismatic geometry with two phenoxo oxygens (O1 and O2) and two methoxy oxygens (O3 and O4) from the ligand, while the remaining six positions are occupied by six oxygens from the three bidentate nitrate

Table 1 Important crystal data for [**L–Cu–Ln**] and [**L–Zn–Ln**] complexes. None of the [**L–Ni–Ln**] complexes could be crystalized as single crystals, suitable for SCXRD studies and therefore do not appear in this table. [**Z1**], [**Z2**] and [**Z3**] are taken from our earlier publication (ref. 16) and given here for comparison

Compound	[C1]	[C2]	[C3]	[C4]	[C5]	[Z1][16]	[Z2][16]	[Z3][16]	[Z4]	[Z5]
Empirical formula	$C_{20}H_{22}N_5O_{13}$ CuNd	$C_{20}H_{22}N_5O_{13}$ CuPr	$C_{20}H_{22}N_5O_{13}$ CuSm	$C_{20}H_{22}N_5O_{13}$ CuDy	$C_{20}H_{22}N_5O_{13}$ CuEr	$C_{23}H_{29}N_4O_{13}$ ZnNd	$C_{23}H_{29}N_4O_{13}$ PrZn	$C_{23}H_{29}N_4O_{13}$ SmZn	$C_{22}H_{25}N_4O_{12}$ ZnDy	$C_{22}H_{25}N_4O_{12}$ ZnEr
CCDC No.	1913571	1891364	2021619	1891363	1891365	1480671	1480672	1480673	1918470	1918455
F. W.	748.17	744.87	754.31	766.46	771.22	792.15	774.77	784.24	1530.66	1540.18
Space group	$P2_1/n$	$P2_1/n$	$P2_1/n$	$P2_1/n$	$P2_1/n$	$P2_1/c$	$P2_1/c$	$P2_1/a$	$P2_1/n$	$P2_1/n$
Cryst. system	Monoclinic	Monoclinic	Monoclinic	Monoclinic	Monoclinic	Monoclinic	Monoclinic	Monoclinic	Monoclinic	Monoclinic
a (Å)	11.8049(9)	11.8416(13)	11.8697(11)	11.7752(5)	11.7498(3)	12.014(5)	12.110(5)	11.436(5)	17.832(3)	17.803(2)
b (Å)	14.7000(11)	14.6648(16)	14.6939(10)	14.6236(6)	14.6319(4)	23.693(5)	23.722(5)	23.800(5)	15.148(2)	15.1306(2)
c (Å)	14.8759(12)	14.8379(17)	14.8613(14)	14.7256(6)	14.6998(4)	11.509(5)	11.489(5)	11.895(5)	20.585(3)	20.604(3)
α (°)	90	90	90	90	90	90	90	90	90	90
β (°)	100.951(3)	101.178(4)	101.230(4)	100.653(2)	100.583(10)	111.885(5)	112.009(5)	111.805(5)	102.116(10)	102.025(2)
γ (°)	90	90	90	90	90	90	90	90	90	90
V (Å^3)	2534.4(3)	2527.8(5)	2542.4(4)	2491.9(2)	2484.2(1)	3039.9(19)	3060.0(2)	3005.9(2)	5436.7(13)	5428.2(12)
T (K)	173.15	110.02	110.0	110.0	100.0	293	293	293	293	293
Z	4	4	4	4	4	4	4	4	2	4
D_{calc} (mg m^{-3})	1.961	1.957	1.971	2.043	2.062	1.700	1.682	1.733	1.870	1.885
μ (mm^{-1})	2.943	2.824	3.201	3.908	4.290	2.545	2.424	2.800	3.678	4.023
GOF on F^2	1.092	1.360	1.360	1.221	1.066	1.049	1.220	1.166	1.059	1.061
$R(F_o^2)^a$	0.0291	0.0325	0.0310	0.0244	0.0194	0.0809	0.0663	0.1067	0.0359	0.0274
$R_w(F_o^2)^b$	0.0664	0.0734	0.0755	0.0526	0.0412	0.1809	0.1167	0.1944	0.0935	0.0705

^{a} $R_1 = \sum||F_o| - |F_c||/\sum|F_o|$. ^{b} $wR_2 = [\sum[w(F_o^2 - F_c^2)^2]/\sum[w(F_o^2)^2]]^{1/2}$.

groups (O5, O7, O8, O10, O11 and O13) as clearly shown in the ORTEP diagrams Fig. 2(a–e). The iso-structurality of [**L–Cu–Ln**] complexes is also supported by their similar coordination environment (Fig. 3(d)) and packing diagram, which have similar packing in all the five complexes presented in Fig. 3(a), whereas respective individual packing diagrams of each complex are presented in ESI,† Fig. S3(a–e).

[**L–Zn–Ln**] complexes fall into two categories. [**Z1–Z3**], which have already been discussed in our previous report,[16] have similar coordination with Zn^{II} ions adopting the distorted square pyramidal geometry, in which the planar positions are occupied by two phenoxo oxygen (O1 and O2) and two nitrogen (N1 and N2) atoms, while the fifth axial position is occupied by the bridged acetate oxygen (O11) atom, Fig. 2(f–h). The Ln^{III} ions with ten coordination number adopt bicapped square antiprismatic geometry. The coordination numbers are fulfilled by ten oxygen atoms; four from the ligand (two phenoxo oxygens (O1 and O2) and two methoxy oxygens (O3 and O4)), while the remaining six oxygens are from two bidentate nitrate units (O5, O7, O8 and O10), one from acetate oxygen (O12) and one from solvent methanolic oxygen (O13) atom as presented in Fig. 2(f–h). These three complexes exhibit a similar coordination environment (Fig. 3(e)) and therefore are expected to have similar packing as presented in Fig. 3(b), whereas individual packing diagrams are presented in ESI,† Fig. S3(f–h). In the other two complexes [**Z4**] and [**Z5**], the Zn^{II} coordination environment is similar to that above, with square pyramidal geometry where the planar position is occupied by two phenoxo oxygen (O1 and O2) along with two nitrogen (N1 and N2) atoms and the fifth axial position is occupied by an acetate oxygen (O11) (Fig. 2(i and j)). Here the Ln^{III} ions are only nine coordinated with capped square antiprismatic geometry as opposed to the ten coordination of the previous series. Four oxygens from the tetra coordinated ligand (two phenoxo oxygens (O1 and O2) and two methoxy oxygens (O3 and O4)) along with two bi coordinated nitrate groups (O5, O7, O8 and O10) and the ninth position is occupied by the acetate oxygen (O12) fulfilling the coordination requirements of the lanthanide ion as presented in the ORTEP diagrams in Fig. 2(i and j). These two have a similar coordination environment (Fig. 3(f)) and are expected to have similar packing as presented in Fig. 3(c), whereas individual packing diagrams are presented in the ESI,† Fig. S3(i and j).

The [**L–Cu–Ln**] complexes have similar interactions as they all have similar coordination environments. Thus [**C1** to **C5**] also have similar packing (Fig. 3) stabilized by C–H···O hydrogen bonding between oxygen atoms of nitrate and hydrogen atoms of the butyl group, aromatic rings and imine group. This weak interaction gives extra stability to the crystal packing. It is to be noted that the interactions in the corresponding series are almost similar, leading to similar packing. In addition to this weak interaction, the [**L–Cu–Ln**] complex also exhibits C···π interactions, which are prominent in the ORTEP representation shown in the last column of Table 3.

On the contrary, [**L–Zn–Ln**] complexes (*i.e.*, [**Z1** to **Z5**]) are also stabilized by intermolecular C–H···O hydrogen bonding between oxygen atoms of nitrate and the hydrogen atoms of the

Table 2 Important bond angles (°), bond lengths (Å) and dihedral angles (°) for [**L–Cu–Ln**] and [**L–Zn–Ln**] complexes. Pictorial depictions of the bond angles and lengths are given below the tabulated data

	Nd		Pr		Sm		Dy		Er	
Metals	Cu	Zn	Cu	Zn	Cu	Zn	Cu	Zn	Cu	Zn
Angles (°)										
N1–M–N2	100.19	96.43	100.47	96.73	100.33	96.86	100.73	96.02	100.85	96.18
N1–M–O3	90.97	88.03	92.28	88.33	90.78	87.55	92.52	87.26	90.89	88.92
O3–M–O2	78.85	77.43	78.87	77.02	79.02	76.43	78.00	75.04	77.58	74.95
O2–M–N1	92.58	86.73	90.93	87.03	92.42	87.14	91.02	88.95	92.67	87.23
O2–Ln–O3	60.65	64.52	60.43	64.32	60.33	65.13	61.83	66.89	62.25	67.26
O3–Ln–O4	62.19	59.46	61.87	59.95	61.85	60.53	63.56	63.52	64.30	63.81
O4–Ln–O1	144.45	134.02	114.81	134.02	114.96	134.03	113.62	143.66	142.97	143.19
O1–Ln–O2	62.20	59.32	61.94	59.64	62.04	59.93	63.36	64.77	63.70	65.27
Distance (Å)										
M–N1	1.958	2.062	2.005	2.048	1.963	2.043	1.960	2.067	1.999	2.055
M–N2	1.997	2.071	1.964	2.057	2.007	2.068	2.000	2.058	1.954	2.065
M–O1	1.938	2.052	1.953	2.038	1.946	2.038	1.938	2.053	1.933	2.057
M–O2	1.943	2.076	1.941	2.075	1.950	2.078	1.935	2.066	1.938	2.063
M–O5	—	1.996	—	2.005	—	1.988	—	2.007	—	2.146
Ln–O1	2.612	2.740	2.619	2.743	2.602	2.725	2.542	2.527	2.526	2.512
Ln–O2	2.406	2.414	2.424	2.402	2.500	2.365	2.409	2.268	2.390	2.285
Ln–O3	2.475	2.422	2.490	2.408	2.432	2.367	2.331	2.312	2.304	2.254
Ln–O4	2.589	2.716	2.595	2.736	2.626	2.731	2.567	2.526	2.542	2.494
Ln–O6	—	2.409	—	2.417	—	2.361	—	2.312	—	2.392
Ln–O7	—	2.520	—	2.520	—	2.362	—	—	—	—
Dihedral angle (N1–N2–O3–O2)	17.345	22.015	17.359	21.562	17.233	21.023	16.353	17.297	15.377	17.222
Six membered ring formation with M (d-block metal)										
Plane angle	26.367	52.494	26.151	52.941	26.055	52.931	25.364	46.316	24.639	46.303
Centroid	3.733	3.649	3.747	3.626	3.751	3.621	3.729	3.676	3.730	3.673

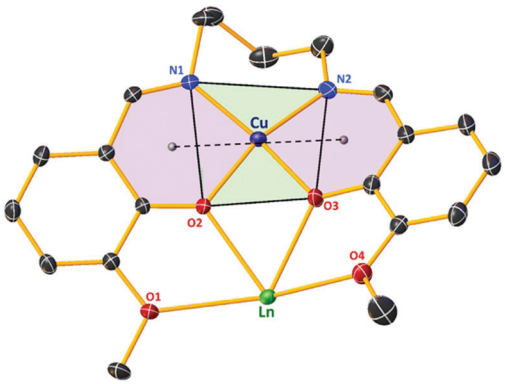

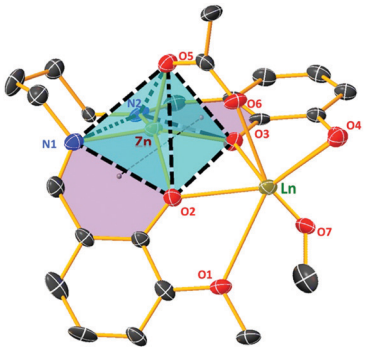

butyl group, imine group, methoxy group, and acetate anion and also coordinated methanol hydrogens of a neighbouring complex moiety (*vide* Table 3). In addition, the crystal structure is further stabilized by C–H···π interactions between the centroids of the methoxy-substituted phenyl rings of neighbouring molecules as tabulated and depicted in Table 3. Here complexes [**Z4** and **Z5**] have different packing because they have two crystallographically independent units, leading to extra stability to the crystal system because of more packing interactions.

Structural determination of [L–Ni–Ln] complexes: powder X-ray diffraction study using Rietveld refinement

The details of powder X-ray diffraction patterns along with Rietveld refined data are shown in Fig. 4 for [**L–Ni–Nd**], while for the rest of the Ni complexes they are presented in the ESI,† Fig. S4. The experimental data are shown as red circles, and calculated intensities are shown as solid black lines. The bottom blue lines represent the difference between the measured and the calculated intensities. The allowed Braggs positions for the space group are marked as vertical green lines. The space groups are: $P2_1/c$ for [**N1**] and [**N2**], $P2_1/a$ for [**N3**] and $P2_1/n$ for [**N4**] and [**N5**]. We have observed that all the experimental peaks are allowed Bragg 2θ positions for the corresponding space group.

In the refinement, the initial parameters were taken from the corresponding [**L–Zn–Ln**] complexes. Parameters such as lattice constants are taken for the monoclinic system, occupancies are kept as 1.0, scale factors, isothermal parameters, and shape parameters have been kept unconstrained. The background has been corrected by pseudo-Voigt function.[13] The refined PXRD patterns show that the samples are in single phase form.

The various R factors are listed in the ESI,† Table S1. The values of R factors such as R_p are found to be large. Similar

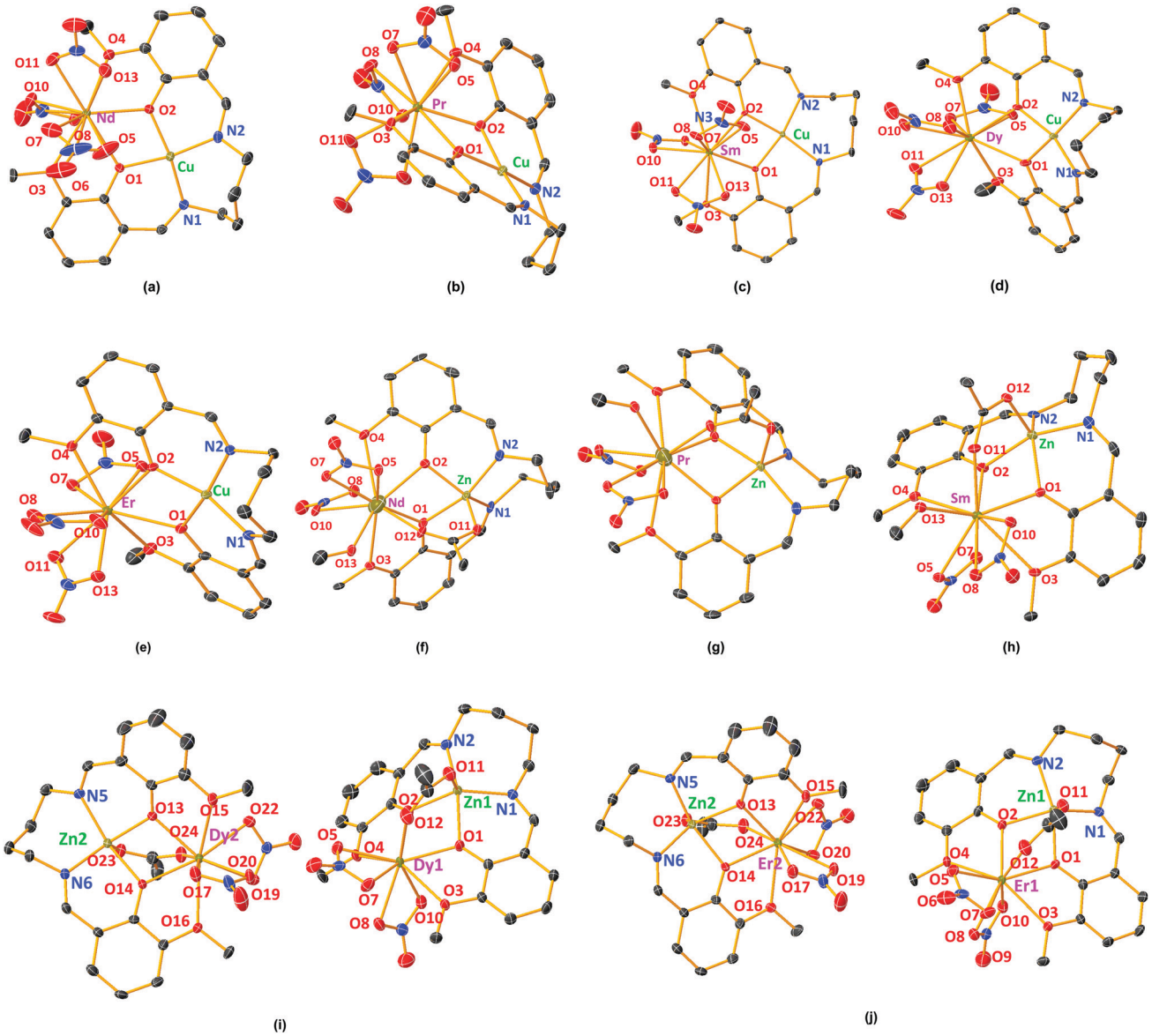

Fig. 2 ORTEP diagrams of [**L–Cu–Ln**] and [**L–Zn–Ln**] complexes at 30% probability ellipsoids. (a) For [**L–Cu–Nd**], [**C1**]: O6 atom is split and one split component is represented for better presentation; (b) for [**L–Cu–Pr**], [**C2**]; (c) for [**L–Cu–Sm**], [**C3**]; (d) for [**L–Cu–Dy**], [**C4**]; (e) for [**L–Cu–Er**], [**C5**]; (f) for [**L–Zn–Nd**], [**Z1**]; (g) for [**L–Zn–Pr**], [**Z2**]; (h) for [**L–Zn–Sm**], [**Z3**]; (i) for [**L–Cu–Dy**], [**Z4**]; and (j) for [**L–Zn–Er**], [**Z5**].

high values of R factors for crystalline materials have been observed by other authors.[25,26] This could be due to the large noise-to-signal ratio of PXRD patterns for crystalline materials. However, we have observed an appropriate (close to 1) value of goodness of fit (χ^2), which justifies the goodness of refinement. In the powder diffraction pattern of crystalline materials, diffuse scattering is more dominant than in those of bulk crystalline materials, and it is due to the large surface to volume ratio of the atoms. The diffuse scattering becomes significant at the nanoscale, while Bragg scattering gets diminished, which leads to a decline in crystallinity and large R factors.[27]

From the derived structure it is found that [**L–Ni–Ln**] structurally follows [**L–Zn–Ln**] complexes, which is also expected from the other experimental data (CHN, PXRD, IR, and photophysical studies). Here in [**L–Ni–Ln**], the Ni ion is found to be in a square pyramidal structure with coordination number of 5 and the lanthanide ion is in a bicapped square antiprismatic geometry with coordination number of 10, which is structurally similar to [**L–Zn–Ln**] complexes. The inset of Fig. 4 shows the structure of the [**L–Ni–Nd**] complexes obtained from PXRD data which is as expected.

Photophysical studies

There is considerable interest in the photophysical properties of lanthanide complexes because of the various fascinating properties as described in the introduction. Particularly, the long-wavelength narrow band with a longer lifetime[28] makes it attractive for many applications like telecommunication and in biology.[4,5] Here, we

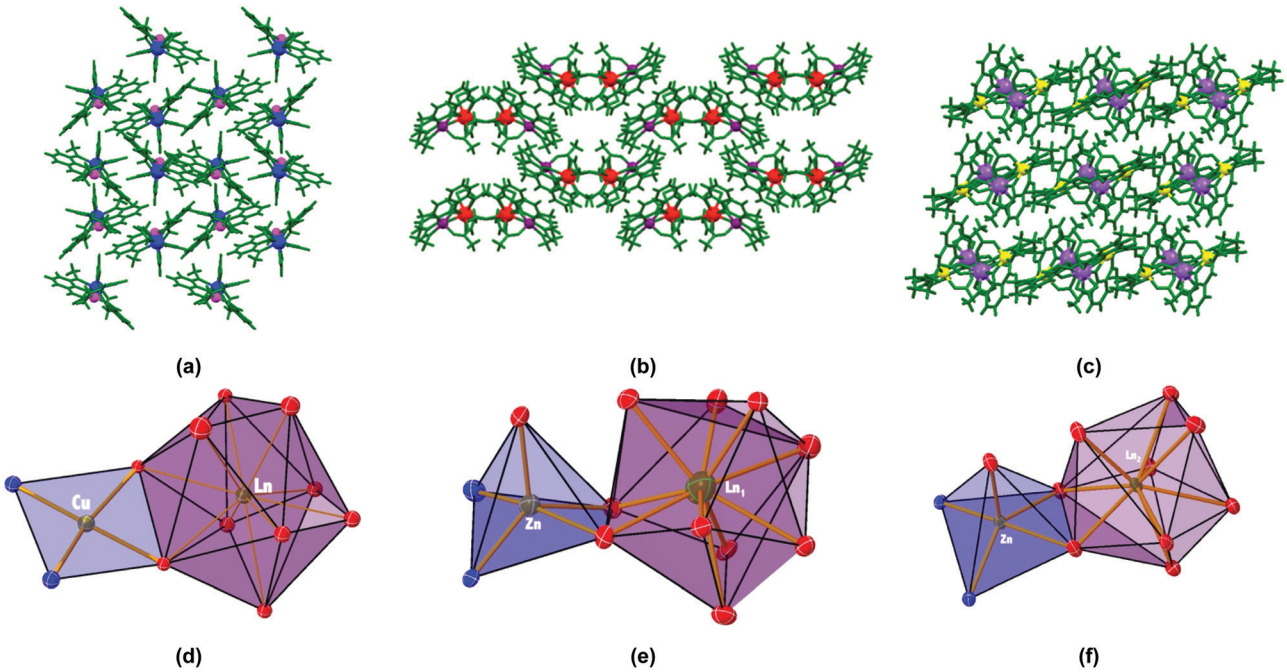

Fig. 3 Packing diagrams of complexes viewed down the a-axis. (a) All [**L–Cu–Ln**] complexes, ([**L–Cu–Nd**] presented here) in this series show the same packing. (b) Packing in [**L–Zn–Nd**], and complexes [**Z1**]–[**Z3**], show the same type of packing. (c) Packing in [**L–Zn–Dy**]:[**Z4**], and [**L–Zn–Er**]:[**Z5**] also shows the same packing. (d–f) Show the polyhedral environment around the metal ions.

Table 3 The important intermolecular π interactions common in the corresponding series. C···π for [**L–Cu–Ln**] complexes and C–H···π for [**L–Zn–Ln**] complexes. The last column shows the ORTEP pictorial representation of the intermolecular interaction

Complex	C···π (Å)	C–H···π (Å)
[**C1**]	3.322	Absent
[**C2**]	3.303	Absent
[**C3**]	3.310	Absent
[**C4**]	3.301	Absent
[**C5**]	3.399	Absent
[**Z1**]	Absent	2.743
[**Z2**]	Absent	2.758
[**Z3**]	Absent	2.729
[**Z4**]	Absent	2.964
[**Z5**]	Absent	3.049

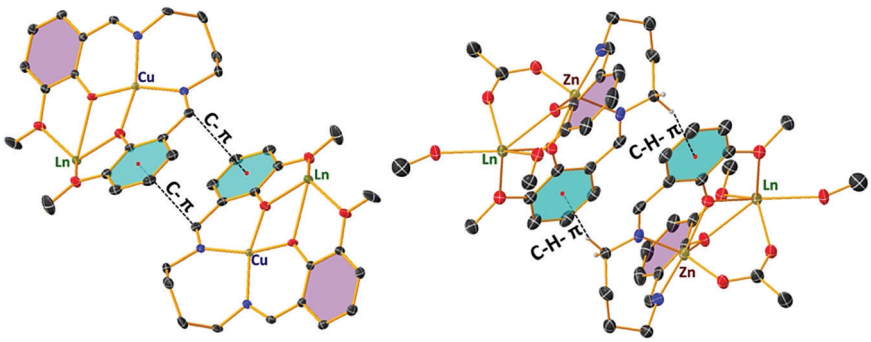

intend to find the effect of d-block metal ion influence on the lanthanide emission. The photophysical properties have been studied in MeOH. The UV-vis absorption spectra of Schiff base ligand (**L**) alone and its complexes [**L–Ni–Ln**], [**L–Cu–Ln**] and [**L–Zn–Ln**] are presented in Fig. 5.

The free ligand exhibits the lowest energy band at 420 nm, in addition to higher energy bands at 221, 260, 292 and 330 nm. While the 420 nm band is assigned to n–π* transitions in the ligand, the higher energy bands are attributed to the π–π* transitions in the benzene ring and azomethine group.[16] Interestingly, all the metal ion complexes show blue-shifted absorption spectra upon complexation. Such blue shifting of absorption bands on Ln–ligand complexation is also reported in the literature.[28] On the other hand, interestingly, we have also come across several reports where redshift is mentioned on complexation.[29] This discrepancy is presumably due to the fact that the dilute solution of lanthanide metal complex does not provide the lowest energy band with appreciable optical density to detect and thereby is missed in spectra published in several reports.[1,4,8,16] All complexes here have displayed three characteristic bands at 229 nm, 274 nm and 353 nm, which are due to intra ligand charge transfer (229, and 274 nm) and ligand to metal charge transfer (353 nm), respectively. However, the d–d transition band in [**L–Cu–Ln**] complexes is not observed at a low concentration (1×10^{-5} M, in Fig. 5a), but at

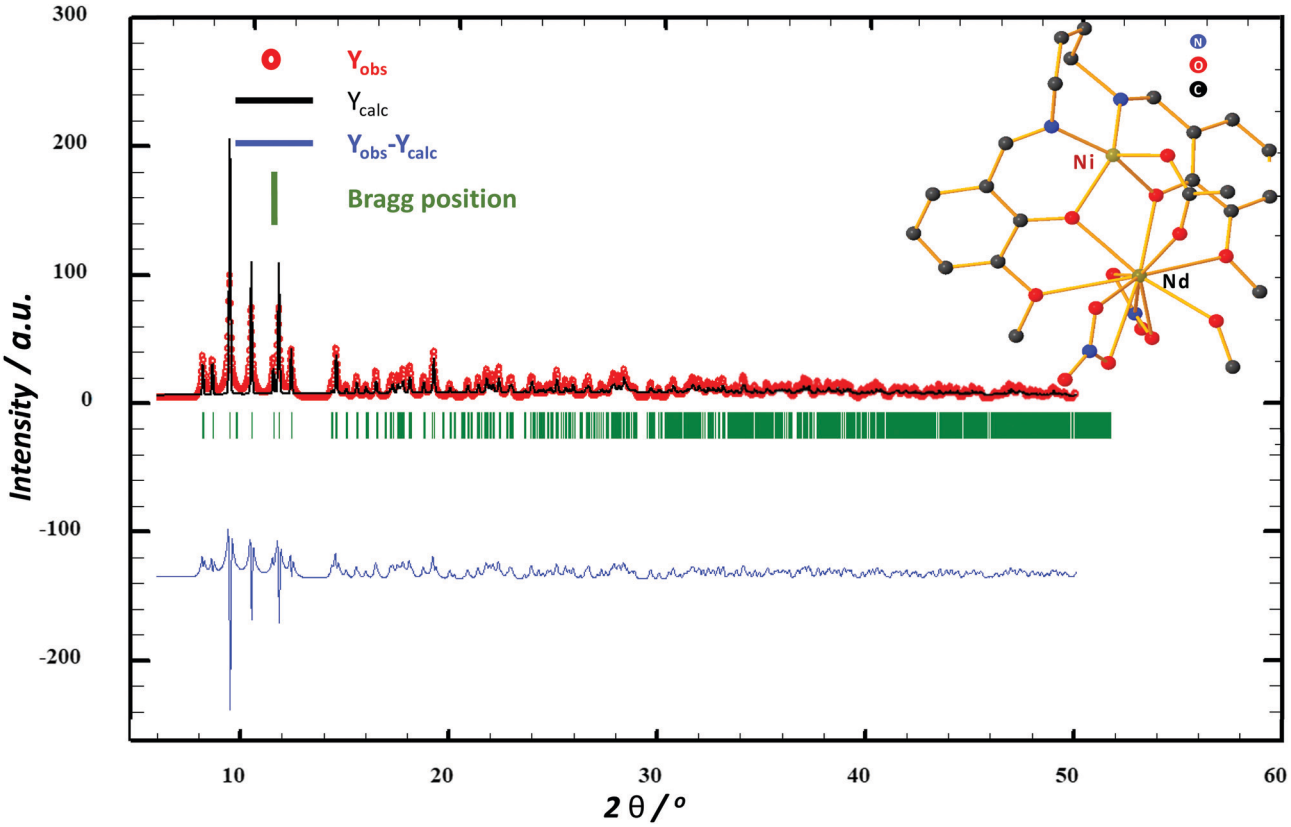

Fig. 4 Rietveld refined XRD patterns for the [**L–Ni–Nd**], [**N1**] complex. The red circles represent experimental points, and the solid black line represents Rietveld refined data. The bottom blue line shows the difference between the experimental and refined data. The marked 2θ positions are the allowed Bragg peaks. The inset shows the expected structure derived from the Rietveld refinement.

a higher concentration ($\sim 2 \times 10^{-4}$ M) this band shows up in the range of 500–800 nm (*vide* ESI,† Fig. S2). On the other hand, [**L–Ni–Ln**] complexes show a prominent d–d transition band at around 420 nm, even at low concentration ($\sim 1 \times 10^{-5}$ M) (Fig. 5b). Ni^{II} is a d^8 system with the electronic configuration $[Ar]3d^9 4s^1$, whereas Cu^{II} is a d^9 system having $[Ar]3d^9 4s^0$ electronic configuration; in both the cases the d orbital is not completely filled and thus under ligand field strength, the d orbital gets split into t_{2g} and e_g energy levels between which transition takes place. Many reports are available for d–d transition in Cu^{II} and Ni^{II}

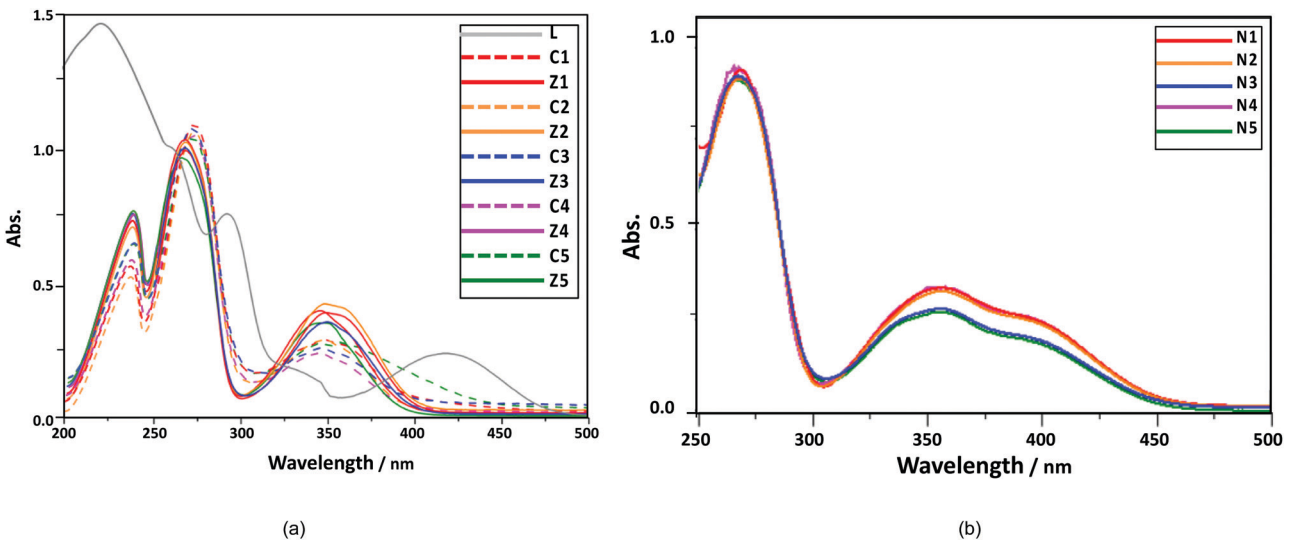

Fig. 5 Absorption spectra for the (a) ligand (**L**) and complexes [**L–Zn–Ln**] (in solid lines) and [**L–Cu–Ln**] complexes (in dotted lines) (at $\sim 1 \times 10^{-5}$ M). (b) Absorption spectra for [**L–Ni–Ln**] complexes, showing the d–d transition band ($\sim 1 \times 10^{-5}$ M).

complexes and their significance.[30] On the other hand, the **[L–Zn–Ln]** complexes did not show any d–d transitions as d^{10} systems (of Zn^{II}) have no inter-electronic transitions between the split d-levels ($t_{2g} \Leftrightarrow e_g$) as they are fully filled.[31] These absorption spectra of lanthanide complexes are found to match well with those of similar complexes reported in the literature.[32]

Recently, attention has also been focused particularly on the complex of Ln^{III} with the near-infrared (NIR) emission (~900–1700 nm), which is transparent for the biological tissues making it possible to be applied in bioassays and bio-luminescent probes.[9] Photophysical properties of Ln^{III} ions depend markedly on their coordination environment that includes chromophore ligands, and d-block metal ions. Emission studies of lanthanide complexes with d-block metal ions, as a sensitizer for Ln emission, are often found to be interesting because their responses can be tuned by varying the ligand, and/or d-block metal ions. Liu and coworkers have made several significant contributions highlighting the interesting luminescence properties exhibited by various types of trinuclear complexes.[32–35] The emission spectra of ligands (**L**) and all the complexes have been studied in methanol and are presented in Fig. 6. The emission spectrum of the ligand exhibits a broad (400–600 nm) emission band with a maximum at 486 nm. The emission spectra of all the complexes exhibit a broad emission band covering 400–600 nm (visible region) with an emission maximum at around 450 nm (for [**L–Zn–Ln**]) which is blue-shifted compared to the free ligands (486 nm). The blue-shift may originate from the ligand-to-metal-charge transfer (LMCT) emission and has already been reported.[14,15] Interestingly, in addition to the ligand centred band, one can observe several sharp emission bands in the visible range for [**L–Zn–Ln**] complexes. These peaks correspond to the f–f transitions. Table 4 tabulates all transition data along with their term symbols and their assignments that could be observed in these complexes. These emission bands are completely absent in Cu and Ni complexes. It is therefore fascinating to observe that despite having Ln ions in these complexes (**C1–C5** and **N1–N5** series), no emission from Ln could be observed. The complete quenching

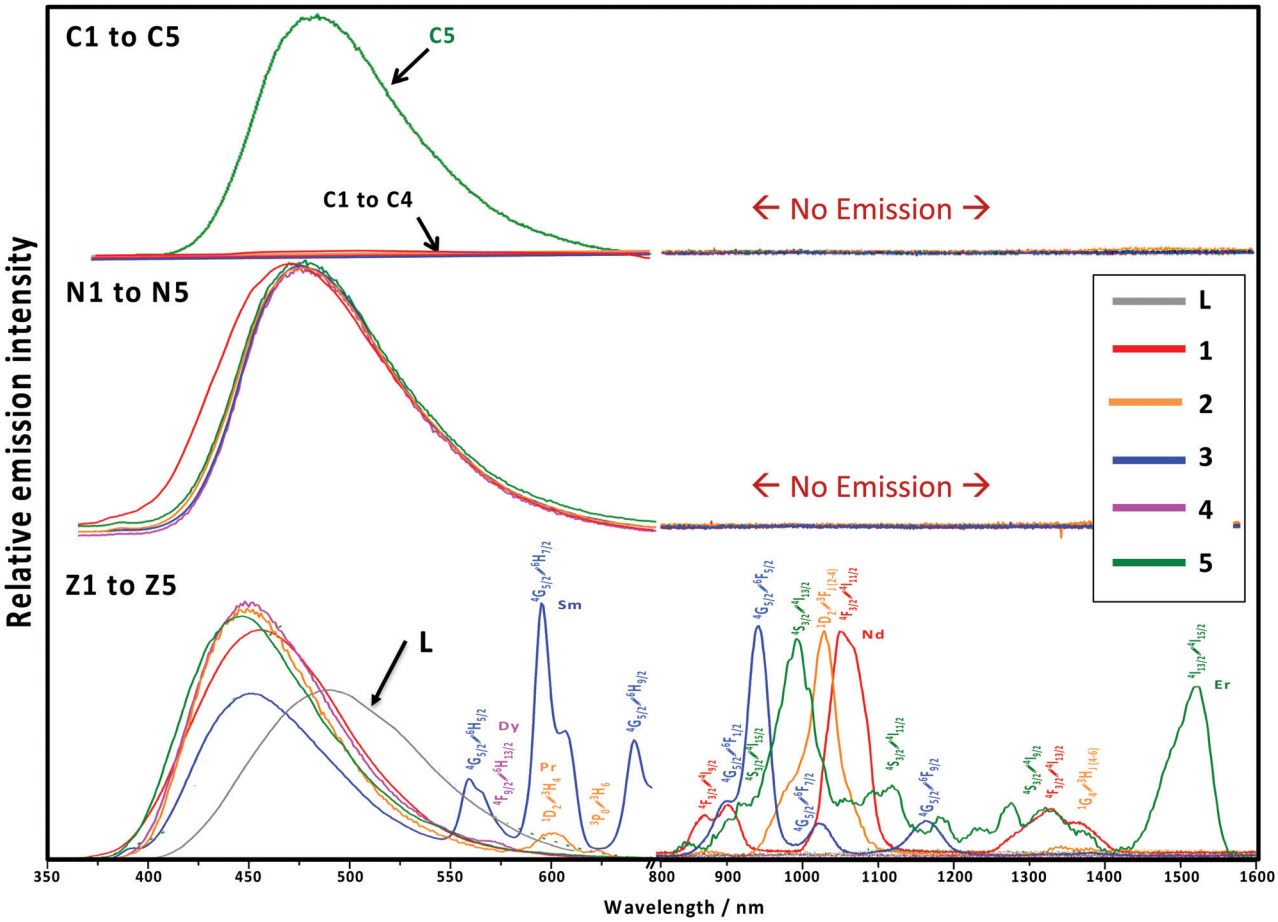

Fig. 6 Emission spectra for bare ligand and complexes. Emission spectra are categorized into groups based on d-block metal ions in the complexes. The top set shows the emission spectra of all Cu-containing Ln complexes (*i.e.*, all the [**L–Cu–Ln**]). The **C5** (corresponds to [**L–Cu–Er**]) shows exceptional behaviour showing a broad emission band in the visible region as discussed in the text. The middle set shows emission spectra of all Ni-containing Ln complexes (*i.e.*, all the [**L–Ni–Ln**]). In both the sets, no emission from the Ln ion is observed. The lower panel shows the emission spectra of all Zn ion-containing Ln complexes (*i.e.*, all the [**L–Zn–Ln**]). Rich emission bands can be observed for the [**L–Zn–Ln**] complexes in the NIR region down to 1600 nm. Assignments for emission bands for Ln ions are also depicted on each peak. The excitation wavelengths were kept at 420 nm and 350 nm for ligand and complexes, respectively.

of emission throughout the range for Cu^{II} complexes (except [**C5**]) is also noteworthy. The exception that the [**C5**] which is an Er^{III} complex (*i.e.*, [**L–Cu–Er**]) only shows emission in the visible region among all Cu^{II} complexes is quite intriguing. However, a thorough literature search indicates the existence of a few reports on such exception, that copper–lanthanide complexes show some exceptional behaviours, particularly with the higher series of lanthanide ions such as Eu, Tb, and Er ions.[36] Ohtsu *et al.* have reported the photophysics of a macrocyclic trinuclear heterobimetallic complex with Eu^{II} (namely, [$EuCu_2L_2(NO_3)\cdot 3MeOH$]) highlighting the quenching of all bands except one around the 720 nm region. They have ascribed the quenching of bands due to the overlap between the lanthanide emission with that of d–d transition in Cu^{II}.[36] While Sakamoto and coworkers have observed only one selective band for Eu^{III} (at 625 nm) and Tb^{III} (at 550 nm),[37] McMohan and coworkers have reported a drastic decrease of intensity for Tb^{III} bands on complexation with Cu^{II}, instead of complete disappearance.[38] Therefore, the selective appearance of any specific band for copper complexes is intriguing and needs further exclusive studies with the help of a time resolved fluorescence technique.

However, all the Ni^{II} complexes [**L–Ni–Ln**], show emission in the visible region but none in the NIR region. On the contrary, all [**L–Zn–Ln**] complexes show emission in the range spanning 400 nm to 1600 nm, having both broad and sharp bands. [**Z5**], an Er^{III} complex [**L–Zn–Er**] exhibits a strong emission band at 1520 nm, longest among all, followed by [**Z2**] and [**Z1**] at 1407 nm and 1333 nm, respectively. The reason for the complete absence of Ln^{III} emission in Cu^{II} and Ni^{II} containing complexes might be related to the existence of d–d transition within the metal complex. It is well-known that in the case of a simple Cu–ligand complex, the fluorescence of a ligand is often seen to be completely quenched.[8] Herein these complexes, d-block metal ion-organic ligand (Cu/Ni/Zn–L) complexes should be the source of energy for transfer to any of the Ln^{III} ion energy manifolds.[1,2,24] Since this [L–Cu/Ni] complex emission gets quenched, there is no energy transfer to Ln^{III} ion energy manifold, making the complex non-emissive in the NIR region. Due to the absence of d–d transition in the [L–Zn] system, [**L–Zn–Ln**] complexes show usual emission in the NIR range. It transpires from this study that [L–Cu] and [L–Ni] are not suitable to function as "antenna" in such complexes while [L–Zn] undoubtedly acts as a superior "antenna". However, questions may arise as to whether the different coordination environment (ten-coordination in the [**L–Cu–Ln**] complex *vs.* nine-coordination in [**L–Zn–Ln**] complexes) affects the photophysics of these complexes. Lanthanide coordination complexes consist of two electronic systems with little interaction between the ligand electronic system and the electronic configuration of the lanthanide ions. The latter consists of 4f electrons which are shielded by the filled $5s^2$ $5p^6$ subshells allowing little mixing between the two systems (the "covalency" of the Ln–ligand bonds rarely exceeds 5%). As a consequence:[39] (a) the absorption/emission spectra of the ligands sustain little changes upon complexation and (b) on the other hand, the absorption/emission spectra of the lanthanide ions (f–f-transitions) will sustain large changes, not in energy (*i.e.* transition occurs more or less at the same wavelengths), but in crystal field splitting and intensity. This is presumably because complexation modifies the symmetry around the metal ion. So it is expected to see some differences depending on the coordination number, but they are sometimes difficult to observe depending on the ion. The shape of absorption spectra for Nd^{III} has been used in the past to determine the

Table 4 Emission data for the complexes. Bands are assigned based on the literature as cited on the top of the code of the complexes

Code	~(400–500)	~(600–700)			~(800–1100)			~(1200–1300)		~(1400–1500)
L	491									
Nd^{III}	Visible				$^4I_{9/2}$–$^4I_{9/2}$	$^4I_{9/2}$–$^4I_{11/2}$			$^4I_{9/2}$–$^4I_{13/2}$	
[**Z1**][1,2,4,5,7,16]	451				870; 904	1057			1333	
[**C1**]	—	No emission								
[**N1**]	474									
Pr^{III}	Visible	$^1D_2$–$^3H_4$	$^3P_0$–$^3H_6$			$^1D_2$–$^3F_4$		$^1G_4$–$^3H_4$	$^1G_4$–$^3H_5$	$^1G_4$–$^3H_6$
[**Z2**][1,5,7,16]	450	600	623			1028		1338	1372	1407
[**C2**]	—	No emission								
[**N2**]	478									
Sm^{III}	Visible	$^4G_{5/2}$–$^6H_{5/2}$	$^4G_{5/2}$–$^6H_{7/2}$	$^4G_{5/2}$–$^6H_{9/2}$	$^4G_{5/2}$–$^6F_{1/2}$	$^4G_{5/2}$–$^6F_{5/2}$	$^4G_{5/2}$–$^6F_{7/2}$	$^4G_{5/2}$–$^6F_{9/2}$		
[**Z3**][1,5,7,16]	452	559	595	641	889	942	1021	1161		
[**C3**]	—	No emission								
[**N3**]	477									
Dy^{III}	Visible	$^4F_{9/2}$–$^6H_{13/2}$								
[**Z4**][1,5,7,11]	450	570								
[**C4**]	—	No emission								
[**N4**]	478									
Er^{III}	Visible				$^4S_{3/2}$–$^4I_{15/2}$	$^4S_{3/2}$–$^4I_{13/2}$		$^4S_{3/2}$–$^4I_{11/2}$	$^4S_{3/2}$–$^4I_{9/2}$	$^4I_{13/2}$–$^4I_{15/2}$
[**Z5**][1,2,5,7,11]	446				917	994		1119	1319	1520
[**C5**]	472	No emission								
[**N5**]	477									

coordination number but found to be not reliable. Depending on the ion, it is reported that a charge transfer band, such as LMCT for Eu and Yb may appear.[40] However, each case is a bit special and generalizations may be incorrect.

Conclusions

Here in this paper, we report three new series of hetrodinuclear d- and f-block metal complexes of Ni^{II}, Cu^{II} and Zn^{II} with f-block Ln^{III} (Nd, Pr, Sm, Dy and Er) metal ions. All ten complexes having Cu/Zn are structurally characterized by SCXRD. In the absence of single crystals for [**L–Ni–Ln**], the structures of Ni containing complexes have been established by PXRD data (Rietveld refinement) and found to be similar to those of [**L–Zn–Ln**] complexes. Crystal packing for all [**L–Cu–Ln**] complexes is similar in which Ln is ten coordinated. However, [**L–Zn–Ln**] complexes show two different types of packing due to variation of the coordination number of Ln^{III} ions (nine or ten). Photophysical studies, however, reveal fascinating differences. While all the [**L–Zn–Ln**] complexes show prominent Ln emission in the visible to NIR range (600 nm to 1600 nm), [**L–Ni–Ln**] and [**L–Cu–Ln**] complexes do not exhibit any emission in the NIR region. Considering the fact that synthesis of metal–ligand–lanthanide complexes has been an attractive field to obtain the NIR emission, which can be used for various purposes, our study clearly demonstrates that one must be careful, while choosing the d-block metal ion. It is now clear that L–Cu and L–Ni do function as ''antenna'', while L–Zn is found to be an excellent antenna for transferring the absorbed energy to Ln energy manifolds.

Conflicts of interest

There are no conflicts to declare.

Acknowledgements

Department of Chemistry, Institute of Science, Banaras Hindu University is gratefully acknowledged for the infrastructure. AV thanks CSIR, New Delhi, for providing a JRF-Fellowship. SSS acknowledges the help in XRD data recording from Prof. H Nishihara and the JSPS Bridge Fellowship.

References

1 J.-C. G. Bünzli, Lanthanide Luminescence For Biomedical Analyses and Imaging, *Chem. Rev.*, 2010, **110**(5), 2729–2755.

2 H. Uh and S. Petoud, Novel Antennae For The Sensitization of Near Infrared Luminescent Lanthanide Cations, *C. R. Chim.*, 2010, **13**(6–7), 668–680.

3 (*a*) S. I. Weissman, Intramolecular Energy Transfer The Fluorescence of Complexes of Europium, *J. Chem. Phys.*, 1942, **10**(4), 214–217; (*b*) J.-C. G. Bünzli and S. Eliseeva, Intriguing Aspects of Lanthanide Luminescence, *Chem. Sci.*, 2013, **4**(5), 1939.

4 (*a*) Y. Li, Y. Sun, J. Li, Q. Su, W. Yuan, Y. Dai, C. Han, Q. Wang, W. Feng and F. Li, Ultrasensitive Near-Infrared Fluorescence-Enhanced Probe for *in Vivo* Nitroreductase Imaging, *J. Am. Chem. Soc.*, 2015, **137**(19), 6407–6416; (*b*) E. S. Levy, C. A. Tajon, T. S. Bischof, J. Iafrati, A. Fernandez-Bravo, D. J. Garfield, M. Chamanzar, M. M. Maharbiz, V. S. Sohal, P. J. Schuck, B. E. Cohen and E. M. Chan, Energy-Looping Nanoparticles: Harnessing Excited-State Absorption for Deep-Tissue Imaging, *ACS Nano*, 2016, **10**(9), 8423–8433; (*c*) G. Jalani, R. Naccache, D. H. Rosenzweig, L. Haglund, F. Vetrone and M. Cerruti, Photocleavable Hydrogel-Coated Upconverting Nanoparticles: A Multifunctional Theranostic Platform for NIR Imaging and On-Demand Macromolecular Delivery, *J. Am. Chem. Soc.*, 2016, **138**(3), 1078–1083.

5 (*a*) J.-C. G. Bünzli, S. Comby, A.-S. Chauvin and C. D. B. Vandevyver, New Opportunities for Lanthanide Luminescence, *J. Rare Earths*, 2007, **25**(3), 257–274; (*b*) J. Andres and A.-S. Chauvin, Lanthanides: Luminescence Applications, *Encycl. Inorg. Bioinorg. Chem.*, 2012, 1–18; (*c*) J.-C. G. Bünzli and S. V. Eliseeva, Lanthanide NIR Luminescence for Telecommunications, Bioanalyses and Solar Energy Conversion, *J. Rare Earths*, 2010, **28**(6), 824–842.

6 J.-C. G. Bünzli, Lanthanide Photonics: Shaping the Nanoworld, *Trends Chem.*, 2019, **1**(8), 751–762.

7 L. Sun and L. Shi, Lanthanides: Near-Infrared Materials, *Encycl. Inorg. Bioinorg. Chem.*, 2012, **1**, 123–133.

8 (*a*) D. Maji, M. Zhou, P. Sarder and S. Achilefu, Near-Infrared Fluorescence Quenching Properties of Copper(II) Ions for Potential Applications in Biological Imaging, Reporters, Markers, Dyes, Nanoparticles, and Molecular Probes for Biomedical Applications VI, 2014; (*b*) Y. Rahimi, A. Goulding, S. Shrestha, S. Mirpuri and S. K. Deo, Mechanism Of Copper Induced Fluorescence Quenching of Red Fluorescent Protein, DsRed, *Biochem. Biophys. Res. Commun.*, 2008, **370**(1), 57–61.

9 Y. Iizumi, M. Yudasaka, J. Kim, H. Sakakita, T. Takeuchi and T. Okazaki, Oxygen-Doped Carbon Nanotubes for Near-Infrared Fluorescent Labels and Imaging Probes, *Sci. Rep.*, 2018, **8**(1), 1–6.

10 (*a*) J.-C. G. Bünzli, On The Design of Highly Luminescent Lanthanide Complexes, *Coord. Chem. Rev.*, 2015, **293–294**, 19–47; (*b*) J. B. S. Linden-Leibeszeit, S. V. Eliseeva, N. Chaudhary, M. Zeller, S. Petoud and E. R. Trivedi, Near-Infrared Emitting Heterobimetallic Zn-4F Schiff Base Complexes With Visible Excitation Wavelength, *Eur. J. Inorg. Chem.*, 2020, 75–78.

11 (*a*) M. Fondo, J. Corredoira-Vázquez, A. Herrera-Lanzós, A. M. García-Deibe, J. Sanmartín-Matalobos, J. M. Herrera, E. Colacio and C. Nuñez, Improving The SMM and Luminescence Properties of Lanthanide Complexes with LnO_9 cores in the Presence of Zn^{II}: An Emissive Zn_2Dy Single Ion Magnet, *Dalton Trans.*, 2017, **46**(48), 17000–17009; (*b*) X. Zhou, J.-L. Peng, C.-W. Wen, Z.-Y. Liu, X.-H. Wang, J.-Z. Wu and Y.-C. Ou, Tuning The Structure And Zn(II) Sensing of Lanthanide Complexes with Two

Phenylimidazophenanthrolines By Acetonitrile Hydrolysis, *CrystEngComm*, 2017, **19**(43), 6533–6539; (*c*) W.-K. Dong, J.-C. Ma, L.-C. Zhu, Y.-X. Sun, S. F. Akogun and Y. Zhang, A Series of Heteromultinuclear Zinc(II)–Lanthanide(III) Complexes Based on 3-Meosalamo: Syntheses, Structural Characterizations, and Luminescent Properties, *Cryst. Growth Des.*, 2016, **16**(12), 6903–6914.

12 J. E. Post and D. L. Bish, *Rietveld Refinement of Crystal Structures Using Powder X-ray Diffraction Data*, Modern Powder Diffraction, 1989, pp. 277–308.

13 W. I. F. David, Powder diffraction peak shapes. Parameterization of the pseudo-Voigt as a Voigt function, *J. Appl. Crystallogr.*, 1986, **19**, 63–64.

14 (*a*) M. A. Spackman and P. G. Byrom, *Chem. Phys. Lett.*, 1997, **267**, 215; (*b*) J. J. McKinnon, A. S. Mitchell and M. A. Spackman, *Chem. – Eur. J.*, 1998, **4**, 2136.

15 N. F. Chilton, R. P. Anderson, L. D. Turner, A. Soncini and K. S. Murray, PHI: A Powerful New Progrm for the Analysis of Anisotropic Monomeric and Exchange-Coupled Polynuclear d- and f- block Complexes, *J. Comput. Chem.*, 2013, **34**, 1164–1175.

16 N. Dwivedi, S. K. Panja, A. Verma, T. Takaya, K. Iwata, S. S. Sunkari and S. Saha, NIR Luminescent Heterodinuclear [Zn^{II} Ln^{III}] Complexes: Synthesis, Crystal Structures and Photophysical properties, *J. Lumin.*, 2017, **192**, 156–165.

17 N. Dwivedi, S. S. Sunkari, A. Verma and S. Saha, Molecular Packing Dependent Solid-State Fluorescence Response of Supramolecular Metal–Organic Frameworks: Phenoxo-Bridged Trinuclear Zn(II) Centered Schiff Base Complexes with Halides and Pseudohalides, *Cryst. Growth Des.*, 2018, **18**(9), 5628–5637.

18 W. I. F. David, Powder diffraction: Least-squares and beyond, *J. Res. Natl. Inst. Stand. Technol.*, 2004, **109**, 107–123.

19 R. Y. Young, *The Rietveld Method*, Oxford University Press, Oxford, 1996.

20 S. Carbonin, F. Martignago, G. Menegazzo and A. Negro, X-ray single-crystal study of spinels: *in situ* heating, *Phys. Chem. Miner.*, 2002, **29**, 503–514.

21 G. M. Sheldrick, A short history of SHELX, *Acta Crystallogr., Sect. A: Found. Adv.*, 2008, **64**(1), 112–122.

22 O. V. Dolomanov, L. J. Bourhis, R. J. Gildea, J. A. K. Howard and H. Puschmann, ''OLEX2: A Complete Structure Solution, Refinement and Analysis Program'', *J. Appl. Crystallogr.*, 2009, **42**, 339–341.

23 G. M. Sheldrick, Crystal Structure Refinemnet with SHELXL, *ActaCrystallogr., Sect. C: Struct. Chem.*, 2015, **71**, 3–8.

24 L. J. Farrugia, WinGX and ORTEP for Windows: an Update, *J. Appl. Crystallogr.*, 2012, **45**, 849–854.

25 Y. M. Abbas, S. A. Mansour, M. H. Ibrahim and S. E. Ali, Microstructure characterization and cation distribution of nanocrystalline cobalt ferrite, *J. Magn. Magn. Mater.*, 2011, **323**, 2748–2756.

26 M. Bhagwat, A. V. Ramaswamy, A. K. Tyagi and V. Ramaswamy, Rietveld Refinement Study of Nanocrystalline Copper Doped Zirconia, *Mater. Res. Bull.*, 2003, **38**, 1713–1724.

27 (*a*) N. G. Jovic, A. S. Masadeh, A. S. Kremenovic, B. V. Antic, J. L. Blanusa, N. D. Cvjeticanin, G. F. Goya, M. V. Antisari and E. S. Bozin, Effect of Thermal Annealing on Structural and Magnetic Properties of Lithium ferrite nanoparticles, *J. Phys. Chem.*, 2009, **113**, 20559–20567; (*b*) B. H. Toby, R factors in Rietveld analysis: How Good is Good Enough?, *Powder Diffr.*, 2006, **21**, 67–70.

28 (*a*) G. A. Kumar, R. E. Riman and J. G. Brennan, NIR Emission From Molecules and Clusters with Lanthanide–Chalcogen Bonds, *Coord. Chem. Rev.*, 2014, **273–274**, 111–124; (*b*) M. Caricato, C. Coluccini, D. A. Vander Griend, A. Forni and D. Pasini, From Red to Blue Shift: Switching the Binding Affinity from the Acceptor to the Donor End by Increasing the Π-Bridge in Push–Pull Chromophores with Coordinative Ends, *New J. Chem.*, 2013, **37**(9), 2792–2799; (*c*) N. Sabbatini, M. Guardigli and J.-M. Lehn, Luminescent Lanthanide Complexes as Photochemical Supramolecular Devices, *Coord. Chem. Rev.*, 1993, **123**(1–2), 201–228.

29 (*a*) O. V. Kotova, S. V. Eliseeva, A. S. Averjushkin, L. S. Lepnev, A. A. Vaschenko, A. Y. Rogachev, A. G. Vitukhnovskii and N. P. Kuzmina, Zinc(II) Complexes with Schiff Bases Derived from Ethylenediamine and Salicylaldehyde: The Synthesis and Photoluminescent Properties, *Russ. Chem. Bull.*, 2008, **57**(9), 1880–1889; (*b*) L. Thunus and R. Lejeune, Overview of Transition Metal and Lanthanide Complexes as Diagnostic Tools, *Coord. Chem. Rev.*, 1999, **184**(1), 125–155.

30 E. Gallo, E. Gorelov, A. A. Guda, A. L. Bugaev, F. Bonino, E. Borfecchia, G. Ricchiardi, D. Gianolio, S. Chavan and C. Lamberti, Effect of Molecular Guest Binding on the d–d Transitions of Ni2+ of CPO-27-Ni: A Combined UV–Vis, Resonant-Valence-To-Core X-Ray Emission Spectroscopy, and Theoretical Study, *Inorg. Chem.*, 2017, **56**(23), 14408–14425.

31 Ł. Czekański, S. K. Hoffmann, P. Barczyński, A. Gąsowska, R. Bregier-Jarzębowska, A. Zalewska, J. Goslar, M. Ratajczak-Sitarz and A. Katrusiak, Crystal Structure and Physical Properties of 1-Methyl-3-(Carboxymethyl)Benzimidazolium Betaine·Cubr2 In Crystal and Water Solution, *New J. Chem.*, 2016, **40**(12), 10526–10535.

32 H.-R. Wen, J.-J. Hu, K. Yang, J.-L. Zhang, S.-J. Liu, J.-S. Liao and C.-M. Liu, Family of Chiral Zn^{II}–Ln^{III} (Ln = Dy and Tb) Heterometallic Complexes Derived from the Amine–Phenol Ligand Showing Multifunctional Properties, *Inorg. Chem.*, 2020, **59**(5), 2811–2824.

33 B. Miroslaw, B. Cristóvão and Z. Hnatejko, Heterometallic Zn^{II}–Ln^{III}–Zn^{II} Schiff Base Complexes with Linear or Bent Conformation—Synthesis, Crystal Structures, Luminescent and Magnetic Characterization, *Molecules*, 2018, **23**(7), 1761–1777.

34 H.-R. Wen, J.-L. Zhang, F.-Y. Liang, K. Yang, S.-J. Liu, J.-S. Liao and C.-M. Liu, Tb^{III}/3d–Tb^{III} Clusters Derived from a 1,4,7-Triazacyclononane-Based Hexadentate Ligand with Field-Induced Slow Magnetic Relaxation and Oxygen-Sensitive Luminescence, *New J. Chem.*, 2019, **43**(10), 4067–4074.

35 H.-R. Wen, P.-P. Dong, S.-J. Liu, J.-S. Liao, F.-Y. Liang and C.-M. Liu, 3d–4f Heterometallic Trinuclear Complexes Derived from Amine-Phenol Tripodal Ligands Exhibiting

Magnetic and Luminescent Properties, *Dalton Trans.*, 2017, **46**(4), 1153–1162.

36 H. Ohtsu, T. Suzuki, H. Ohtsuka, A. Ishii and M. Hasegawa, The Unprecedented Role of a Cu^{II} Cryptand in the Luminescence Properties of a Eu^{III} Cryptate Complex, *Monatsh. Chem.*, 2009, **140**(7), 783–787.

37 S. Masatomi, Y. Joji, M. Akira, N. Yuzo and O. Hisashi, Effect of Some d-Transition Metal Complexes of Salen-Type Ligands and Acetylacetone on Fluorescence of Europium(III) and Terbium(III), *Bull. Chem. Soc. Jpn.*, 1994, **67**(10), 2707–2711.

38 (*a*) B. K. McMahon and T. Gunnlaugsson, Lanthanide Luminescence Sensing of Copper and Mercury Ions Using an Iminodiacetate-Based Tb(III)-Cyclen Chemosensor, *Tetrahedron Lett.*, 2010, **51**(41), 5406–5410; (*b*) J. Plotzitzka and C. Kleeberg, [(NHC)Cu^{I}–ER_3] Complexes (ER_3= $SiMe_2Ph$, $SiPh_3$, $SnMe_3$): From Linear, Mononuclear Complexes to Polynuclear Complexes with Ultrashort Cu^{I}—Cu^{I} Distances, *Inorg. Chem.*, 2016, **55**(10), 4813–4823.

39 J.-C. G. Bünzli, Lanthanide Photonics: Shaping the Nanoworld, *Trends Chem.*, 2019, **1**(8), 751–762.

40 J.-C. G. Bünzli, *Lanthanide Luminescence: From A Mystery to Rationalization, Understanding, and Applications*, Including Actinides, 2016, pp. 141–176.

41 B. Kharediya, M. Shukla, S. Saha and S. Sunkari, Influence of Metal to Ligand Molar Ratios on the Supramolecular Structure Formation of Cu(II) with diaminopropane and Iodide: Synthesis, Structure, Spectroscopic and DFT Studies, *J. Mol. Struct.*, 2014, **1062**, 158–166, DOI: 10.1016/j.molstruc.2014.01.021.

42 N. Dwivedi, S. K. Panja, Monika, S. S. Sunkari and S. Saha, Anion Directed Structural Diversity in Zinc Complexes with conformationally Flexible Quinazoline Ligand: Structural, Spectral and Theoretical Studies, *Dalton Trans.*, 2016, **45**, 12053–12068, DOI: 10.1039/c6dt02139e.

43 S. S. Sunkari, B. Kharediya, S. Saha, B. Elrez and J.-P. Sutter, Chain of dimers to assembly of trimers: Temperature and ligand influenced formation of novel supramolecular assemblies of Cu(II) with isomeric (aminomethyl) pyridines and azide, *New J. Chem.*, 2014, **38**, 3529–3539, DOI: 10.1039/c4nj00374h.